Article

Identification Of A New Role Of miR-199a-5p As Factor Implied In Neuronal Damage: Decreasing The Expression Of Its Target X-Linked Anti-Apoptotic Protein (XIAP) After SCI.

Teresa Muñoz-Galdeano [1], David Reigada [1], María Gamarra [2], Altea Soto [1], Maria Asunción Barreda-Manso [1], Irene Novillo [1], Manuel Nieto-Díaz [1] and Rodrigo M-Maza [1,*]

[1] Molecular Neuroprotection Group, Research Unit, National Hospital for Paraplegics (SESCAM), 45071 Toledo, Spain; tmunozd@sescam.jccm.es (T.M.-G.); dreigada@sescam.jccm.es (D.R.); alteasotoneira@gmail.com (A.S.); mbarreda@sescam.jccm.es (M.A.B.-M.); inovilloa@externas.sescam.jccm.es (I.N.); mnietod@sescam.jccm.es (M.N.-D.)

[2] Laboratory of Local Translation in Neurons and Glia. Achucarro Basque Center of Neuroscience; Leioa, Spain; maria.gamarra@achucarro.org (M.G.)

* Correspondence: rodrigom@sescam.jccm.es (R.M.M.)

Abstract: Altered expression of microRNAs (miRNAs) after spinal cord injury (SCI) has been described as being responsible for the main secondary responses, such as apoptosis. X-linked inhibitor apoptosis protein (XIAP) is a key apoptotic component involved in the progression of apoptotic programmed cell death. Several regulators have been described to modulate the XIAP's function, including the post-transcriptional regulator's miRNAs. The main aim of the present work is to identify miRNAs with altered expression after SCI which can regulate XIAP expression using bioinformatics and prediction algorithms. Our bioinformatic analyses identified several miRNAs candidates whose up-regulation following SCI could be responsible for the down-regulation of XIAP, including miR-199a-5p. We examined the relationship between miR-199a-5p and XIAP and their negative correlation expression levels after SCI and characterized the spatial distribution of miR-199a-5p in uninjured and rat-contused spinal cords, using a specific fluorescent *in situ hybridization* (FISH) probe for miR-199a-5p. Finally, *in vitro* simulation of the increment in miR-199a-5p observed after SCI by transfection of a miR-199a-5p mimic into C6 cells confirmed the decrease in XIAP protein levels.. These findings provide new insights into apoptotic miRNAs-mediated mechanisms after SCI, which will help us develop therapeutic strategies based on miRNAs for treating SCI.

Keywords: spinal cord injury; apoptotic cell death; XIAP; neuroprotection; miRNA-based therapies

1. Introduction

Spinal cord injury (SCI) is a complex pathological condition that results in an abnormal or total absence of motor and sensory functions and that leads to devastating physical and social consequences for patients worldwide [1,2]. The damage derived from a traumatic SCI starts with a primary injury due to the direct contusion, laceration, or/and compression, inducing cell death, mainly by necrotic processes. After that, the injury progresses towards a second phase that includes diverse pathological processes such as excitotoxicity, oxidative stress, or exacerbated immune response. This noxious environment leads to further structural and functional alterations that spread neural cell death spatial and temporally from the initial trauma site to the neighbor cells [3]. In this phase, the main form of neural cell death is apoptosis, a programmed cell death highly regulated [4], promoted by both internal and external stimuli. Apoptosis is favored by the alteration of the gene expression balance [5,6], including the up-regulation of pro-apoptotic proteins such as caspases, and the down-regulation of anti-apoptotic proteins such as Bcl-2 family and the inhibitor of apoptosis protein family (IAPs) [7,8]. The human IAP family consists of 8 members and it is defined by the presence of the baculoviral inhibitory repeat (BIR), a

 doi:10.20944/preprints202212.0020.v1

highly conserved ~70 amino-acid sequence [9]. Although all members of this family possess these BIR domains, only cIAP1, cIAP2, and XIAP show anti-apoptotic activity [10]. The IAP family members have several cytoprotective functions and their downregulation after injury makes neural cells more susceptible to cell death processes [11,12]. Through the binding of XIAP´s domains, this anti-apoptotic factor has shown the most potent activity to prevent cell apoptosis by inhibiting the processing, activation, and maturation of the initiator caspase-9 and the effector caspases-3 and -7 [13,14]. Even though the endogenous XIAP is not required for the survival of neurons under physiological conditions [15], its downregulation or knock-out makes neurons more vulnerable to multiple apoptotic triggers [16–20]. XIAP, but not other members of the IAP family -such as cIAP-1 and cIAP-2-, becomes cleaved in the first days following SCI, which has been linked to caspase activation and increased risk of apoptosis of neural cells [20,21]. In previous works, we have demonstrated that SCI causes a reduction in XIAP protein levels, specifically at 3 days post-injury [22]. It has been also shown that the overexpression of XIAP protein is sufficient to prevent neuronal cell death following SCI, axotomy, cerebral ischemia [11], and hypoxia [23]. Therefore, all these data suggest that XIAP protein serves as a natural "safety brake" that can restrict neural death in traumatic or pathological situations.

In addition, SCI induces changes in epigenetic regulators of gene expression such as miRNAs (miRNAs) [24,25]. The miRNAs are short (19-25 nt) non-coding RNA sequences, involved in the regulation of cell physiological and pathophysiological mechanisms, including cell proliferation or death [26–32]. Studies from our group and other laboratories have shown the dysregulation of miRNA expression following traumatic SCI including those that regulate programmed cell death proteins [33–35]. The incremented miR-711 expression after SCI is associated with downregulation of the pro-survival protein Akt [36], whereas decreases in miR-27a may facilitate programmed cell death by allowing expression of pro-apoptotic Bcl-2 family proteins such as Noxa, Puma, and Bax [37]. XIAP expression is also shown to be regulated by miRNAs in a variety of cell types and pathological conditions. Liu et cols. observed that downregulation of miR-192-5p up-regulates the expression of XIAP, decreasing the apoptosis of nerve cells, and promoting the repair and regeneration after sciatic nerve injury [38]. Similarly, Siegel´s study showed that the downregulation of miR-23a is associated with a reduction in cell death after cerebral injury by increasing XIAP levels and the subsequent decrease in caspase activation [39].

The main aim of the present work was to identify miRNAs with altered expression after SCI which can regulate XIAP expression. We obtained several miRNA candidates and validated *in vitro* miR-199a-5p as a post-transcriptional regulator of XIAP as well as the expression changes of both miR-199a-5p and XIAP in an *in vivo* SCI model. These results provide new insights into the role of miR-199a-5p in neural cell death after SCI.

2. Results

2.1. miR-199a-5p is a potential regulator of XIAP expression.

Using *in silico* strategies, we searched for miRNA candidates with miRNA response elements (MREs) in the mRNA sequence of rat XIAP, including the 3'UTR, 5'UTR, and the coding regions. Combining data obtained from four different miRNA target prediction algorithms (TargetScan, miRanda, miRWalk and miRMap) (Figure 1A), we found that only six miRNAs are predicted by all four tools: miR-181a-5p, miR-181b-5p, miR-181c-5p, miR-199a-5p, miR-21-5p, and miR-340-5p. The MREs for all these miRNAs are located in the 3'UTR region (3'UTR-XIAP) but neither in 5'-UTR nor in the coding region.

Preprints (www.preprints.org) | NOT PEER-REVIEWED | Posted: 1 December 2022 doi:10.20944/preprints202212.0020.v1

A.

B.

		miRMap	microRNA.org	TargetScan		miRWalk
	MRE	Score	Score	T.C. score	Aggr. PTC	Score
miR-181a-5p	34	-0.12		-0.19	0.74	0.92
miR-181b-5p	34	-0.1		-0.19	0.74	0.92
miR-181c-5p	34	-0.12		-0.19	0.74	0.92
miR-199a-5p	425	-0.22	-0.3727	-0.18	0.4	0.92
miR-21-5p	324	-0.12	-0.7546	-0.17	<0.1	0.86
miR-340-5p	232	0.04	-0.1064	-0.03	N/A	0.84

C.

	Site	Seed	ΔG_{duplex}	$\Delta\Delta G$
mFold	434	8:1:0	-19.60	-11.26
	452	8:1:1	-19.27	-8.91
	126	8:1:1	-10.6	-2.22
miRMap	425	-	-14.1	-11.14

Figure 1. Selection miRNAs with predicted MREs in the rat 3'-UTR-XIAP. **A.** Venn diagram representing the number of miRNAs predicted by each of four algorithms (TargetScan 8.0, miRanda, miRWalk and miRMap); or by more than one. Six miRNAs candidates were predicted by all four algorithms: miR-181a-5p, miR-181b-5p, miR-181c-5p, miR-199a-5p, miR-21-5p and miR-340-5p. **B.** The table shows the miRNAs selected and the prediction scores calculated by each algorithm. miR-199a-5p (highlighted in blue) is the miRNA that accomplishes the established requirements to continue the study. **C.** Localization of the different MREs for miR-199a-5p in the rat 3'UTR-XIAP whole sequence, indicating the free energy (ΔΔG) score for miRNA-MRE interactions, computed as the free energy gained by transitioning from the state in which the miRNA and the target are unbound (ΔG open) and the state in which the miRNA binds its target (ΔG duplex), according to mFold algorithm.

The prediction scores obtained from each algorithm reflected that miR-199a-5p, miR-181a-5p, and miR-181b-5p showed the highest scores (Figure 1B). However, since previous works have already validated XIAP as a target of miR-181a-5p and miR-181b-5p [40], we focused our efforts on the validation of miR-199a-5p as a regulator of XIAP expression. We evaluated the probability of binding miR-199a-5p to MREs in the sequence of the mRNA of XIAP by studying their folding and accessibility scores with the mFold algorithm [41] (Figure 1C). This algorithm predicted three potential miR-199a-5p MREs in the 3'UTR-XIAP. Among them, the MRE starting in the nt 434, counted from the stop-codon of XIAP mRNA, has the most favorable accessibility score (ΔΔG = -11.26 kcal/mol) (Figure 1C), matching the folding and accessibility scores predicted by miRMap algorithm scores.

2.2. miR-199a-5p targets the 3'UTR-XIAP sequence

To validate the effective binding of miR-199a-5p to the 3'UTR-XIAP, we first carried out luciferase reporter assays. For this purpose, the wild-type and mutated 3'-UTR-XIAP were cloned downstream of the Luciferase reporter gene in the pmiR-GLO vector. There

Preprints (www.preprints.org) | NOT PEER-REVIEWED | Posted: 1 December 2022 doi:10.20944/preprints202212.0020.v1

was an absence of luciferase activity in C6 cells transfected with pmiRGLO° plasmid and with or without co-transfection with miR-199a-5p mimic, discarding any effect of endogenous miRNAs or miR-199a-5p on the plasmid expression. Then, C6 cells were co-transfected with i) either the wild type (pmiRGLO^{XIAP}) or the mutant (pmiRGLO$^{XIAP\text{-}MUT}$) plasmid, and (ii) either the miR-199a-5p or the negative control mimics. As shown in Figure 2, co-transfection of miR-199a-5p mimic significantly reduces the luciferase activity of pmiRGLO^{XIAP} plasmid (34.96 ± 7.13% reduction), compared to co-transfection with the negative control mimic (luciferase/Renilla ratios: pmiRGLO^{XIAP} + miR199a-5p mimic = 61.69 ± 4.4; pmiRGLO^{XIAP} + Neg. Ctrl mimic = 100.23 ± 12.3; t_2 = 12.06 in paired t-test, p-value = 0.0034, n=3). Conversely, transfection with miR-199a-5p mimic does not cause any reduction of pmiRGLO$^{XIAP\text{-}MUT}$ luciferase activity (1.0 ± 1.1%), compared to co-transfection with the negative control mimic (luciferase/Renilla ratio: pmiRGLO$^{XIAP\text{-}MUT}$ + miR199a-5p mimic = 128.47 ± 10%; t_2 = 0.12 in paired t-test, p-value = 0.46, n = 3) which confirms the specificity of miR-199a-5p regulation on the predicted binding site of the 3'-UTR-XIAP.

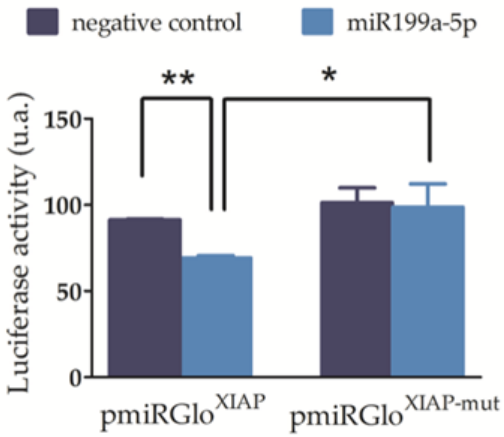

Figure 2. miR-199a-5p effectively binds to the 3'-UTR-XIAP and reduces luciferase reporter gene expression. A. Luciferase reporter assay after co-transfection of C6 cells with (i) either pmiR-Glo-3'-UTR-XIAP (pmiRXIAP) or (ii) either pmiRGLO-3'UTR-XIAP-mut (pmiRXIAP-mut), with miR-199a-5p or negative control mimics. Bar graph summarizes firefly/Renilla emission ratio normalized versus double negative control (empty pmiRGLO° + negative control mimic). Bars represent mean ± SEM of n = 3 independent experiments. **p-value* > 0.05; ***p-value* < 0.01.

2.3. Increased levels of miR-199a-5p reduce XIAP protein expression

To confirm the effect of miR-199a-5p on XIAP expression, we transfected C6 cells with miR-199a-5p or negative control mimics for 24 h, and evaluated both mRNA and protein levels by RT-qPCR and immunoblot assays, respectively. RT-qPCR data showed no statistically difference in XIAP mRNA levels (t_4 = 0.074; p-value = 0.47 in paired t-test; n = 3) (Figure 3A). However, immunoblots showed that miR-199a-5p significantly down-regulated the level of endogenous XIAP protein (33 ± 4.25% reduction; t_4 = 3.296 in a paired t-test; p-value = 0.03; n = 5) (Figure 3B-C). Taken together, the data suggest that overexpression of miR-199a-5p mediates a reduction of endogenous XIAP protein levels via translational repression without degradation of the mRNA.

XIAP immunofluorescence experiments revealed the same trend after cell transfection with the miR-199a-5p mimic (Figure 3D). C6 cell cultures transfected with miR-199a-5p or negative control mimics for 24 h were assayed for endogenous XIAP fluorescence staining intensity level per cell showed a significant reduction of the mean fluorescence after miR-199a-5p transfection compared to negative control mimic transfected cells (Gaussian distribution mean ± SD: Negative control 89.55 ± 36.2; miR-199a-5p mimic 50.25 ± 21.81; t_2=3.327, p-value = 0.039 in a t-test; distribution values from about 3000 cells / per condition) (Figure 3E).

Preprints (www.preprints.org) | NOT PEER-REVIEWED | Posted: 1 December 2022 doi:10.20944/preprints202212.0020.v1

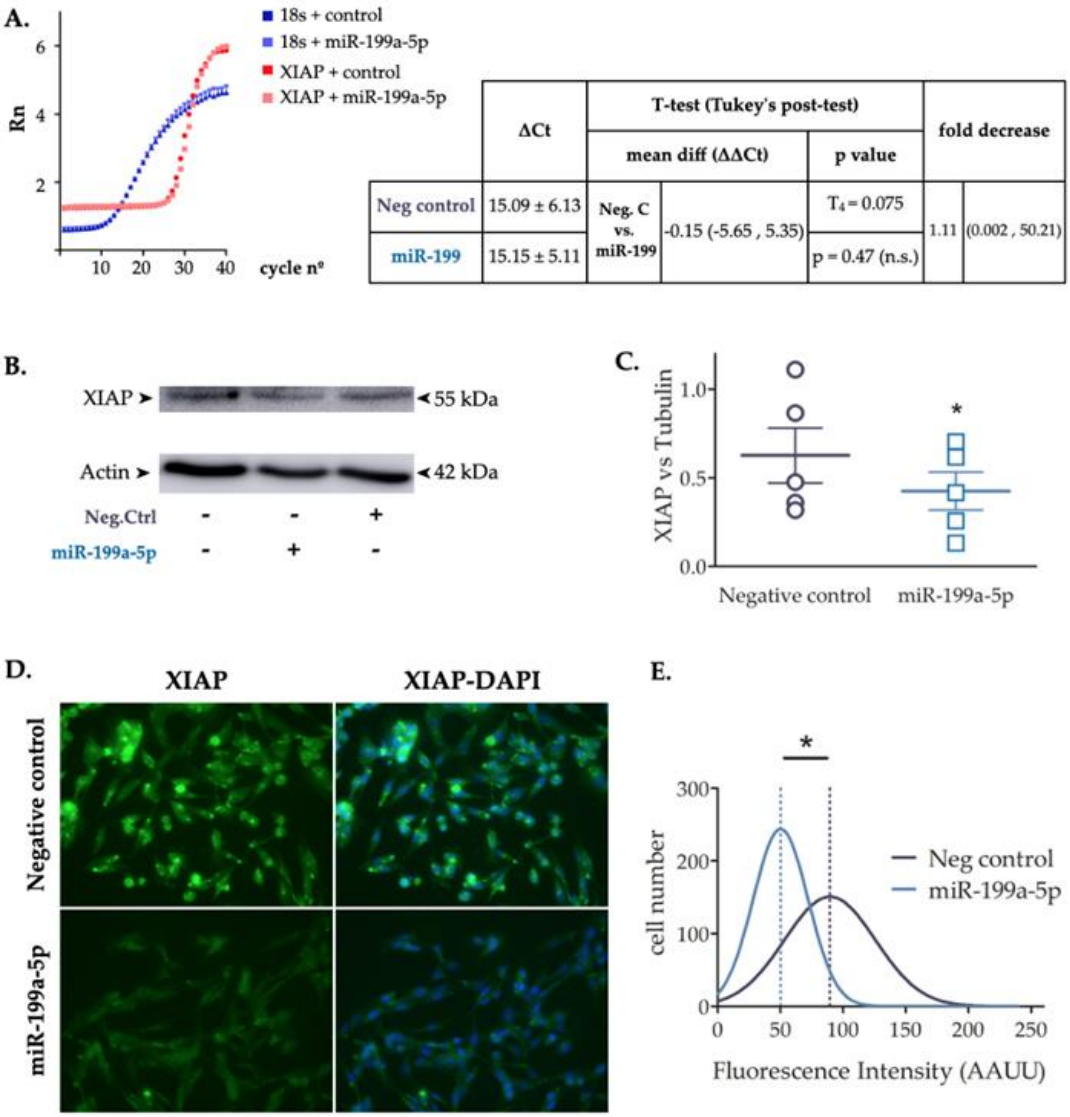

	ΔCt	T-test (Tukey's post-test)			fold decrease	
		mean diff (ΔΔCt)		p value		
Neg control	15.09 ± 6.13	Neg. C vs. miR-199	-0.15 (-5.65 , 5.35)	$T_4 = 0.075$	1.11	(0.002 , 50.21)
miR-199	15.15 ± 5.11			p = 0.47 (n.s.)		

Figure 3. XIAP is a target of miR-199a-5p in C6 cells**. A.** RT-qPCR graphic representing fluorescent values from each probe vs cycle numbers. RT-qPCR results revealed no changes in XIAP gene expression of C6 cell cultures after transfection with miR-199a-5p versus negative control. The table also depicts the statistical analysis of RT-qPCR results, employing a Student's t-test. Representative western blot of expression levels of XIAP in protein samples extracted from C6 cells 24 h after transfection with either miR-199a-5p or negative control mimics (**B)** and dot plot summary **(C)** of the band densitometry. Data were normalized by beta-actin levels for each sample; *p-value < 0.05 (paired t-test; n = 5 independent cell culture preparations) (lines represent mean ± SEM of n=5 independent experiments). **D.** Immunofluorescence assay of XIAP expression in non-transfected control, and negative control or miR-199a-5p mimic transfected C6 cells, labeled with a specific XIAP antibody (green) and DAPI (nuclei staining, blue). Bar scale = 100 μm. **E.** The graph shows the Gaussian distribution of fluorescence intensity of XIAP staining of approximately 3000 cells per condition of C6 cells transfected with negative control (black line) or miR-199a-5p mimics (grey line); *p-value < 0.05 (Student´s t-test; n=2 independent experiments with 5 images per experiment and analyzing approximately 300 cells per image. Dotted line represents the mean fluorescence value for each distribution).

2.4. The increased miR-199a-5p expression after SCI correlated with XIAP downregulation.

From our previously published SCI microarray expression data [42] (GSE19890) and others [30,32,43] shows that, among all the above-predicted candidates, only miR-199a-5p expression is increased at 3 and 7 dpi. To confirm these results, the expression of miR-

Preprints (www.preprints.org) | NOT PEER-REVIEWED | Posted: 1 December 2022 doi:10.20944/preprints202212.0020.v1

199a-5p and XIAP was studied by RT-qPCR from spinal cord samples of non-injured and injured rats at 3 and 7 dpi (n = 3 animals per group). Expression of miR-199a-5p was strongly increased due to the injury (One-way ANOVA, $F_8 = 4.15$, p-value = 0.07) (Figure 4A), being maximum at 3 dpi (1.11 fold increase vs. non-injured animals, Tukey post-hoc test, p-value = 0.08) and returning to control levels at 7 dpi. On the other hand, although the global effect of the injury is not statistically significant (ANOVA; $F_8 = 2.61$, p-value = 0.15) (Figure 4B), XIAP expression inversely correlates with the miR-199a-5p expression change at 3 dpi, with a tendency to decrease (Tukey post-hoc test, p-value = 0.057), and also returning to non-injured levels at 7 dpi (Figure 4C).

A.

	ΔCt	One-Way ANOVA	Tukey's post-test			fold increase	
				mean diff (ΔΔCt)	p value		
0 DPI	15.05 ± 0.0.78	$F_8 = 4.15$ p-value = 0.07 (n.s.)	3 DPI vs 0 DPI	-1.11 (-2.94,0.71)	p = 0.08 (n.s.)	2.158	(0.61,7.67)
3 DPI	13.93 ± 1.0		7 DPI vs 0 DPI	-0.58 (-2.41,1.24)	p = 0.15 (n.s.)	1.49	(0.42,5.31)
7 DPI	14.46 ± 0.63		7 DPI vs 3 DPI	0.53 (-1.29,2.36)	p = 0.2 (n.s.)	0.69	(0.19,2.44)

B.

	ΔCt	One-Way ANOVA	Tukey's post-test			fold decrease	
				mean diff (ΔΔCt)	p value		
0 DPI	14.33 ± 0.62	$F_8 = 2.61$ p-value = 0.15 (n.s.)	3 DPI vs 0 DPI	0.79 (-0.27,1.87)	p = 0.057 (n.s.)	0.57	(0.27,1.2)
3 DPI	15.134 ± 0.19		7 DPI vs 0 DPI	0.37 (-0.69,1.45)	p = 0.21 (n.s.)	0.77	(0.36,1.55)
7 DPI	14.71 ± 0.39		7 DPI vs 3 DPI	-0.42 (-1.49,0.65)	p = 0.037 (*)	1.33	(0.63,2.8)

C.

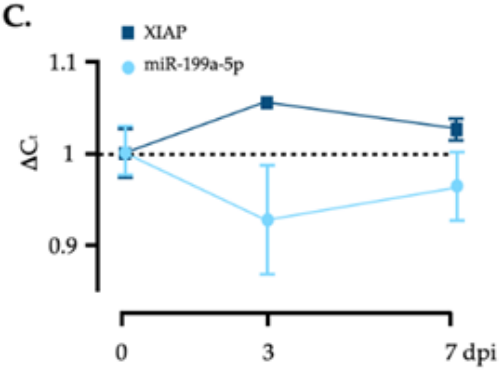

D.

Adjusted R Sq	Df	F value	p-value
0.708	2 and 5	9.502	0.0198

	Df	Estimate	Std. Error	t value	Pr(>t)
Intercept	1	19.748	1.124	17.564	1.1×10^{-5} ***
miR-199a	1	-0.326	0.075	-4.306	0.0076 **
dpi	1	-0.042	0.022	-1.953	0.108

Figure 4. XIAP expression changes after SCI negatively correlate with miR-199a-5p expression levels. Tables **A.** and **B.** summarize the RT-qPCR data of miR-199a-5p and XIAP gene expression respectively, in spinal cord samples at 3 and 7 dpi (n = 3 animals per group with 3 technical replicates each). Also, it reflects the results of statistical analysis of the effect of dpi on gene expression, employing a one-way-ANOVA and Tukey´s Post hoc. **C.** Dot plot graph summarizes the changes in expression levels (ΔCt) of miR-199a-5p and XIAP at 3 and 7 dpi (data were normalized against non-injured rat samples, dotted line. Symbols represent mean ± SEM. Both genes were measured from samples extracted from the same spinal cord sample. **D.** Correlation between the expression of miR-199a-5p and its protein target, XIAP. The analysis shows the linear model adjusted to the dependency of XIAP expression with miR-199a-5p levels after SCI. Results of study revealed a model in which both miR-199a-5p expression and days post-injury significantly determine XIAP expression.

Fitting these results to a linear model, we confirmed that miR-199a-5p expression levels after SCI contribute significantly to about 57% of the total variance of XIAP expression (Adjusted R-squared = 0.5715; $F_{1,6} = 10.34$; p-value = 0.018) (Figure 4D). In addition, although was not statistically significative ($F_1 = 3.102$; p-value = 0.153 in a one-way ANOVA), the linear model fitting showed that the time after injury effect also contributed, in about 70%, of the variance of XIAP expression (Adjusted R-squared = 0.7084; $F_{2,5} = 9.502$; p-value = 0.018; n = 3 animals per group).

Preprints (www.preprints.org) | NOT PEER-REVIEWED | Posted: 1 December 2022 doi:10.20944/preprints202212.0020.v1

2.5. miR-199a-5p is expressed mainly in neurons of spinal cord.

Spatial, temporal, and cellular distribution of miR-199a-5p was evaluated using fluorescence *in situ* hybridization assay (FISH) in non-injured and 3 and 7 dpi rat spinal cords. In the non-injured state, we noticed heterogenous miR-199a-5p staining in the tissue, being mostly expressed in the gray matter (Figure 5A). miR-199a-5p expressing neurons quantification revealed that only 10-20% of neurons located in laminae I to III expresses miR-199a-5p in comparison with the 75-85% of positive neurons in ventral laminae, being 81.11% of these ventral horn neurons located on the VIII and IX Rexed´s laminae (Figure 5B)- (see Table 2). Besides neurons, we also quantify the number of miR-199a-5p expressing neural cells in the white matter, finding that about 25% of neural cells were positive for this miRNA (see Table 1).

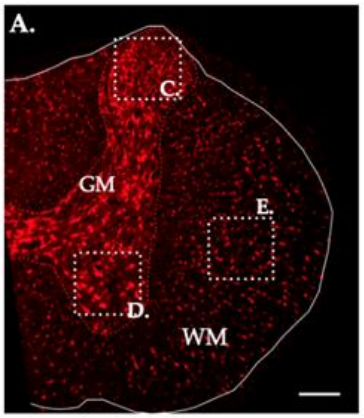

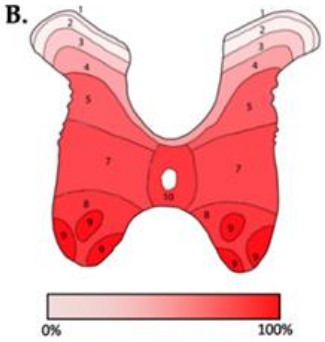

LAMINAE	% Positive miR-199a-5p neurons
I	7.52
II	5.97
III	21.81
IV	37.80
V	67
VII	74.72
VIII	80.66
IX	82.92
X	73.49

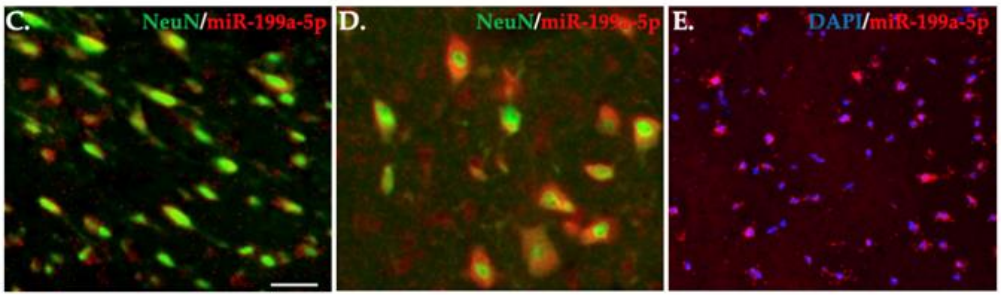

Figure 5. A. Representative immunofluorescence (IF) images of coronal sections of non-injured spinal cords showing miR-199-5p expression. White line trace delimits the spinal cord and red dotted trace delimits white matter to grey matter. **B.** Map of the Rexed laminae in the T9 spinal segment detailing the mean percentage of miR-199-5p positive neurons present in each lamina of the naive spinal cord (6-7 sections from 2 individuals). **C–E.** High-magnified confocal images of the different areas indicated in (A) showing miR-199-5p co-expression with cellular markers for neurons (NeuN) (C-D) and white matter neural cells stained with DAPI (E). Abbreviations in (A) correspond to: GM, grey matter; WM, white matter. Scale bars correspond to 200 μm in (A) to 25 μm in (C–E).

2.6. SCI increases the percentage of neurons and neural cells expressing miR-199a-5p.

Accordingly with the results described from RT-qPCR analysis following SCI, we also sought to localize the areas of the damaged spinal tissue and the spinal cells where these changes occur after SCI. We quantified the percentage of neural cells in the white matter expressing miR-199-5p, after 3 and 7 dpi. The analysis detected a non-statistically significant increase in the percentage of neural cells expressing miR-199a-5p compared to the undamaged spinal cord, especially at 3 dpi in the penumbra area (0.5 mm in both at rostral and caudal directions from the epicenter), and returning to control values at 7 dpi (Figure 6A-C; See Table 2).

Preprints (www.preprints.org) | NOT PEER-REVIEWED | Posted: 1 December 2022 doi:10.20944/preprints202212.0020.v1

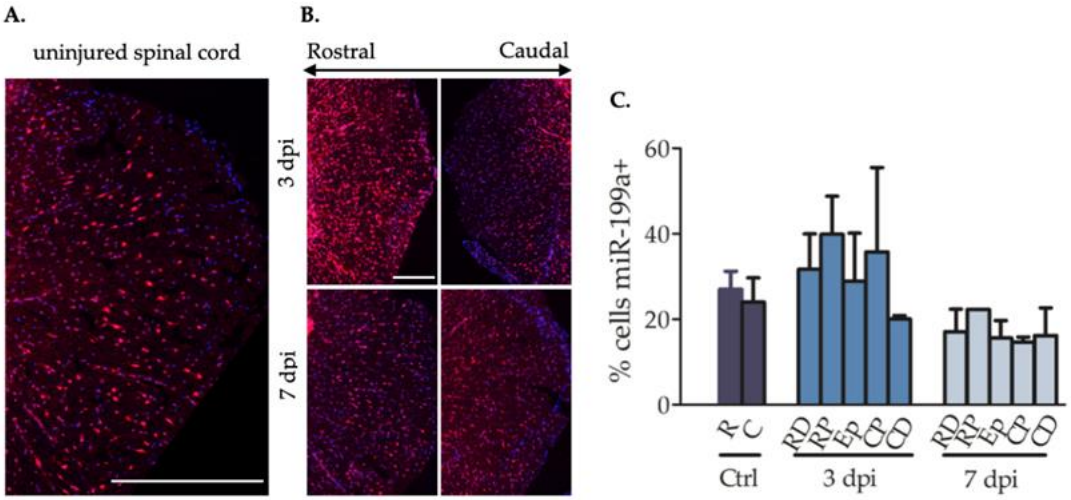

Figure 6. Expression of miR-199-5p in the undamaged spinal cord and after SCI in neural cells of spinal cord white matter. **A.** Detailed representative immunofluorescence image of coronal hemisection of non-injured spinal cords showing miR-199-5p FISH staining (red) and nucleus (blue) from the neural cells of the white matter. Scale bar: 250 μm. **B.** Spatio-temporal distribution of miR-199-5p expression in neural cells from injured spinal cords. Representative immunofluorescence images of coronal hemisections of spinal cords labeled with miR-199-5p probe by FISH assay. Hemisections illustrate miR-199a-5p expression at increasing times after injury (top to bottom) and at 0.5 mm from injury epicenter at both rostral (left) and caudal (right) directions. **C.** The graphic summarizes the percentage of positive miR-199a-5p neural cells (Bars represent mean± SEM). Abbreviations correspond to: R, rostral; C, caudal; RD, rostral distal; RP, rostral proximal; Ep, epicenter; CP, caudal proximal; CD, caudal distal. For each individual (*n*=2), we analyzed 3–4 sections at increasing distances rostral and caudal to the injury epicenter (0.5-1 mm) in non-injured, 3 and 7 dpi. Scale bar: 250 μm.

Table 1. Spatial distribution of neural cells expressing miR-199a-5p in uninjured and after SCI.

Neural cells	non-injured	3 dpi	7 dpi
Rostral (-0.5 mm from epicenter)	27 ± 4.2%	39.86 ± 8.9	22.34 ± 5.3
Caudal (+0.5 mm from epicenter)	24.01 ± 5.67%	35.79 ± 19.72	14.68 ± 1.21

Besides neural cells, no changes were observed in the neurons of the dorsal horn neither at 3 nor 7 dpi (Figure 7A-B). However, in the ventral horn, the percentage of positive neurons increased in a non-statistically significant way at 3 dpi, returning again to non-injured levels at 7 dpi (3 dpi vs 7dpi: $T_{10} = 1.82$; p-value = 0.049; n = 2)(Figure 7D-E).

Preprints (www.preprints.org) | NOT PEER-REVIEWED | Posted: 1 December 2022 doi:10.20944/preprints202212.0020.v1

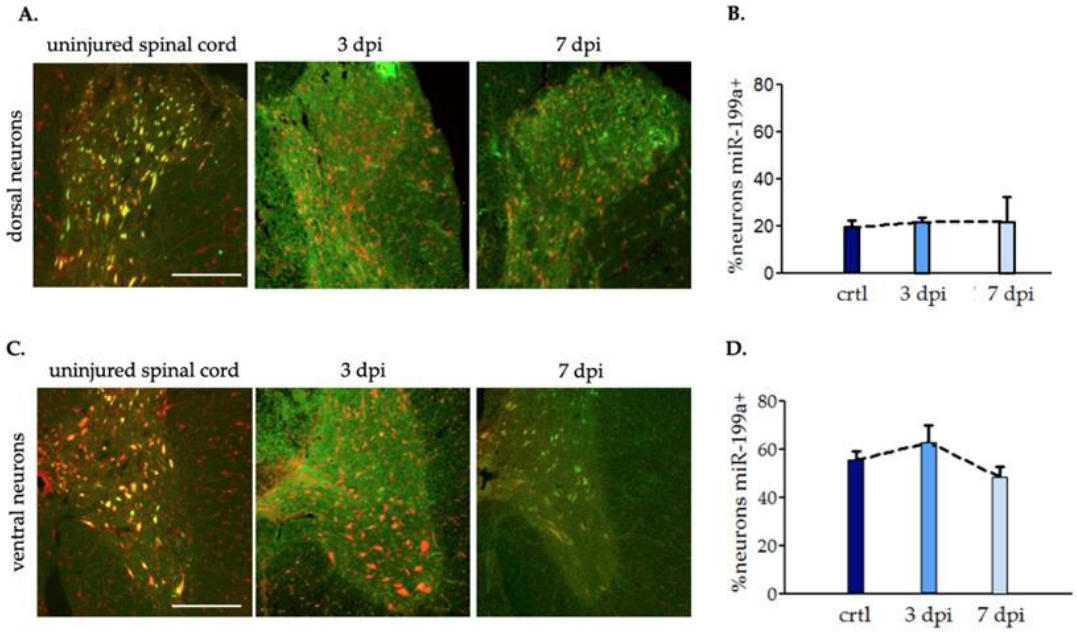

Figure 7. Expression of miR-199-5p in neurons of undamaged and injured spinal cord. **A.** Detail of the dorsal horn (A) and ventral horns (C) of the gray matter of uninjured (left) and 3 dpi (middle) and 7 dpi (right) showing miR-199a-5p (red) and anti-NeuN (green) labeling. Graphic bars summarizes the percentage of positive miR-199a-5p neurons from dorsal (B) and ventral horns (D) (Bars represent mean ± S.E.M, in a minimum of 4 sections per injury condition (n=2)). Scale bar: 250 μm.

Table 2. Neurons expressing miR-199a-5p in dorsal and ventral horn in uninjured and after SCI.

Neurons	non-injured	3 dpi	7 dpi
Dorsal horn	19.22 ± 3.13%	21.53 ± 1.82%	22.04 ± 10.94%
Ventral horn	55,36 ± 3.61%	62.74 ± 7.15%	48.27 ± 4.38%

3. Discussion

Spinal cord injury (SCI) causes an alteration of miRNA post-transcriptional regulation of key gene expression involved in the damaging secondary cascade of events leading to cell demise [42–46]. Apoptotic cell death is a major event that affects neural cells in the secondary injury which is triggered by the unbalance of pro- and anti-apoptotic regulators [47]. Our previous studies and others showed a down-regulation of the anti-apoptotic protein XIAP and upregulation of the caspase activation in the first days after SCI, increasing the risk of apoptosis of neural cells [20,22,48]. In the current study, we have shown for the first time that miR-199a-5p directly regulates the anti-apoptotic protein XIAP expression and that up-regulation of miR-199a-5p following SCI is negatively correlated with XIAP expression levels. We also described the spatial distribution pattern of miR-199a-5p expression in neurons of the grey matter and in neural cells of the white matter, and as one of the most significant findings from this work, the spatio-temporal changes in its expression after SCI. miR-199a-5p belongs to a highly conserved miRNA family of two members, miR-199a-5p and miR-199b [49,50], specifically expressed in nerve tissues [51] and present in human and mouse species [52,53]. Our qualitative analyses described homogeneous miR-199a-5p staining in the spinal cord white matter cells with an alteration of the percentage of miR-199a-5p labeled-positive cells at 3 days after SCI. Conversely, a heterogeneous miR-199a-5p expression in the neuronal cell population of the rat spinal cord is observed, with the higher percentage of neurons expressing miR-199a-5p mostly concentrated in the ventral horn and low or absence of expressing sensory neurons located in the dorsal Rexed's laminae I-IV. Interestingly, after SCI, the percentage of miR-199-5p-expressing neurons is reduced only in the ventral area of the injured spinal cord. These findings agree with an uneven miRNA expression pattern in the näive spinal cord as well as the expression pattern changes described following SCI of the neuronal-specific of the

 doi:10.20944/preprints202212.0020.v1

neuronal-specific miR-138-5p [33], miR-124 [54] or the miR-21 [55]. These results are confirmed by our miR-199a-5p RT-PCR expression data, showing an upregulation following 3 dpi. However, the miR-199a-5p expression changes in the damaged spinal cord may depend on the injury model studied, as described for other miRNAs expression changes after SCI (e.g. up-regulated [56] vs down-regulated miR-21 [57]). Up-regulation of miR199a-5p is observed either in contusive injury (figure 4A and [58]) or in neurotoxicity induced models [59,60], but a miR-199a-5p down-regulation is observed in an ischemia-reperfusion model [61]. Thus, these differences in miRNA expression may account for distinct RNA-based therapeutic applications.

Our validation of a direct regulation of XIAP expression by miR-199a-5p may have a functional impact on the triggered processes of the secondary damage after SCI such as apoptotic cell death. Our bioinformatic studies identified a total of six miRNAs candidates as regulators of XIAP, of which the down-regulated miR-340-5p and some miR-181 family members have been related to the treatment of SCI [62–64]. On the other hand, the up-regulation of miR-21a-5p may have a protective effect on neurons after SCI by the regulation of PDCD4/caspase-3 pathway [55]. Emerging evidence has shown that miR-199a-5p plays a neuroprotector role in several neurological disorders, including SCI, through regulating proteins involved in cell death or survival pathways. The inhibition of miR-199a-5p protected neurons against apoptosis and ROS generation due to over-expression of its protein target Brg1 in a cerebral ischemia/reperfusion injury model [65] as well as induced cerebral ischemic tolerance in the rat brain by the up-regulation of Sirt1 [23]. Similarly, employing ischemic stroke models, down-regulation of miR-199a-5p protected neuron cells against apoptosis and increased cell viability via the CAV-1/MEK/ERK axis [66] as well as improved cognitive function and decreased neuronal apoptosis in hippocampus by activating the AKT signaling pathway [67]. The neuroprotective action of miR-199a-5p has also been reported in SCI. Gao and colleagues described that down-regulation of miR-199a-5p may mediate the beneficial therapeutic effects of olfactory ensheathing cells on SCI rats [58] and the negative effect of increment of miR-199a-5p due to neurotoxicity-induced at the spinal cord was alleviated by employing antagomiRs against miR-199a-5p, suggesting a potential strategy to ameliorate SCI [67]. Our work and other works have described an increased bulk expression of miR-199a-5p in the spinal cord after SCI [58,61] that is negatively correlated with a decrease in XIAP expression [22][20,21]. Although the administration of miR-199a-5p mimic significantly reduces protein XIAP expression level in cell cultures, it does not seem to affect transcript abundance. This observation is not surprising, as it has already been shown that miR-24-mediated repression of XIAP levels is not mediated by mRNA degradation [68]. The miRNA-mediated gene silencing can occur at least mRNA degradation or translation repression, or an interplay of both [69]. Thus our results suggest that miR-199a-5p can exert its negative repression through translation repression rather than by mRNA degradation.

4. Materials and Methods

4.1. Bioinformatics and data mining

We used an in silico screening approach, combining computational tools that employ existing databases and prediction algorithms, and data mining for gene expression data analysis, to predict miRNAs (miRNAs) candidates with microRNA response elements (MREs) in the 5′-UTR and 3′-UTR and the coding region of the mRNA of XIAP and that can be used as therapeutic tools reducing SCI-induced cell death. We used the following four prediction tools: microRNA (http://www.microrna.org), Target Scan (http://www.targetscan.org), miRMap (https://mirmap.ezlab.org/), and miRWalk (http://mirwalk.umm.uni-heidelberg.de/). Although different authors have cautioned against combining predictions because a reduction of sensitivity [70,71], they all acknowledge that these combinations result in enhanced specificity [70]. Already validated miRNA-target interactions were explored using miRTarBase 6.0 database (http://mirtarbase.mbc.nctu.edu.tw/php/index.php; last accessed March 14th, 2020). We chose miR-199a-5p as our main candidate because it was predicted by all 4 tools and the

 doi:10.20944/preprints202212.0020.v1

targeting on XIAP has not been validated yet. We further studied target site accessibility or how likely the MRE of the mRNA of XIAP is accessible to miR-199a-5p binding. We used: i) mFold tool [72] to calculate the free energy of the binding site in comparison with the free energy of the 100 nucleotides flanking the 3′-UTR at both 5' and 3′ sides, and ii) miRMap program to calculate the minimal free energy as a measurement of accessibility, computing stability degree of miRNA-mRNA duplexes.

4.2. Spinal cord injury model

In vivo procedures were performed in female Wistar rats (of 200 g of weight (12–14 weeks of age; RRID:RGD_13508588.). Animals were bred at the animal facility of the Research Unit and housed in plastic cages in a temperature and humidity-controlled room maintained on a 12:12 h reverse light/dark cycle with free access to food and water. SCI surgery followed the methodology described in Yunta and col. [24]. Briefly, following thoracic vertebra 8 (T8) laminectomy, rats were injured by a 200 KDyne contusion (IHSpinal Cord Impactor device from Precision System & Instrumentation, Lexington, KY, USA). After surgery, animals were maintained by daily manual bladder expression and by administration of the analgesic Buprenorphine (0.03 mg/Kg Buprex; Reckitt Benckiser Pharmaceuticals Limited, Richmond, VA, USA), and the antibiotic enrofloxazine (0.4 mg/Kg Baytril; Bayer AG, Leverkusen, Germany) up to 2 days after injury. Hind limb paralysis after injury was confirmed 2 days after the surgery using the Basso, Beattie, and Bresnahan 21-point locomotor score for rat models of SCI (BBB; [73]). We used a BBB value of 7 at 2 days after injury (dpi) as the upper limit to include the animals in the gene expression analyses. We distributed animals in three experimental groups, 3 and 7 dpi and non-injured control, each comprising three individuals. Animals were randomly distributed in the experimental groups following this procedure: each animal received an arbitrary number and was allocated to one of the experimental groups or a reserve group using a random sequence generated with www.random.generator. The first three animals in the sequence were allocated to the control group, the second three to the 3 dpi group, the following three individuals formed the7 dpi group, and the remaining individuals were ordered according to the random sequence to be employed as reserve individuals. The first reserve individual replaced one individual from the 7 dpi group that was excluded because of a suboptimal contusion reflected in an excessive locomotion recovery -above 7 in the BBB scale at 2 dpi, according to the settled exclusion criterion. Animals were subjected to surgeries on different days so that all could be sampled on the same day.

The size of each group was established to be enough to guarantee sufficient statistical power but avoiding unnecessary replications. After the experiment, we employed the obtained gene expression data to confirm this assumption, evaluating whether the agreed upon sample size was enough to reach a power level above 0.95 and a significance level below 0.05. Power calculations were performed a posteriori, that is, after conducting the experiments and gathering the data. To estimate statistical power, we employed the post hoc (a posteriori) analysis of G*Power 3.1 [74] to calculate Cohen's effect size from the group size (3), the mean values for each group, and the average standard deviation. We employed the F test: Fixed effects ANOVA – one way routine of g-power software to calculate the Cohen's effect size index f from the data about group size, number of groups, the mean value for each group, and average standard deviation. Parameters employed were number of groups = 3, sample size = 3/group, significance level = 0.05, estimated effect size = Cohen's f. Data on mean values and average standard deviation are detailed in Figures 2b and c for each gene under analysis. Using these values, we estimated an effect size of f = 1.85271 and a power = 0.9696938 for the miR-199a-5p expression data, and an effect size of f = 4.167007 and a power = 0.9977818 for XIAP expression data. All manipulations and treatments were carried out in full accordance with the guidelines on the care and management of animals established by the European Union (directive 86/609/CEE), the guidelines on the use of animals for Neuroscience Research of the Society for Neuroscience, the NIH guide for the care and use of laboratory animals, and the normative R.D. 1201/2005 10-10 from the Spanish Ministry of the Environment and the

 doi:10.20944/preprints202212.0020.v1

Agriculture Council of the Castilla-La Mancha animal ethics committees. All procedures were approved by the Hospital Nacional de Parapléjicos Animal Care and Use Committee (153BCEEA/2016). All efforts were made to minimize suffering as well as the number of animals used.

4.3. Cell culture

The C6 rat brain glioma cell line (cat#: CRL-2266, RRID:CVCL_0194, ATCC, Manassas, VA, USA,) was grown in RPMI-1640 medium (Gibco) supplemented with 10% fetal bovine serum (FBS; Gibco), 100 U/ml penicillin/streptomycin (Gibco) and 1x glutamine (Gibco). Cells were cultured in a humidified incubator at 37°C in a controlled atmosphere containing 5% CO2. The specific culture plates and cell densities and counts used in each experimental setting are described in their corresponding methodological section.

4.4. Transfections and sample collection

Transfection was carried out according to the recommended procedures by Dharmafect-4 reagent manufacturer (https://dharmacon.horizondiscovery.com/uploadedFiles/Resources/basic-dharmafect-protocol.pdf). In brief, cell cultures were transfected for 24 h with either 50 nM of miR-199-5p mimic (miRBase accession number: MIMAT0000231; miRIDIAN hsa-miR-199a-5p mimic, Dharmacon cat#: C-300533-03-0002, mature sequence: 5′-cccaguguucagacuccuguuc) or a negative control, the cel-miR-67-3p mimic from C. elegans, that has minimal sequence identity with any human, mouse, or rat miRNAs (miRBase accession number: MIMAT0000039; miRIDIAN miRNA mimic negative control #1, Dharmacon cat#: CN-001000-01-05; mature sequence: 5′-ucacaaccuccuagaaagaguaga) (Dharmacon).

4.5. RT-PCR

To carry out RT-qPCR on spinal cord samples, animals were sacrificed by sodium pentobarbital overdose at the defined times (0, 3, or 7 dpi). One cm long spinal cord fragments centered in the injury area were extracted (approximately 70 mg). Samples were coded by a member of the laboratory that did not participate in the RT-qPCR so that all subsequent processes were blinded for the researchers in charge of analyzing the samples. C6 cells (10^6 cells) were plated in 35 mm dishes. After reaching 80% confluence, cultures were transfected for 24 h with 50 nM either miR-199a-5p or negative control mimics. Total RNA samples of spinal cords and C6 cultures were extracted using the Qiazol Lysis Reagent (Qiagen) followed by purification using the miRNeasy Isolation Kit (Qiagen, cat#217004) according to manufacturer protocols. RNA content in each sample was determined using an ND 1000 spectrophotometer (NanoDrop Technologies INC). To determine miR-199a-5p expression, 10 ng of total RNA was reverse-transcribed and amplified using TaqMan miRNA gene expression-specific probe (TaqMan® miRNA assay #000498, Applied Biosystems) following the manufacturer's protocols. The U6 small nuclear RNA served as an internal control (U6 probe TaqMan® miRNA assay #001973, Applied Biosystems). To evaluated mRNA of XIAP content, 1 ug of total RNA was treated with DNase I (Roche) for 30 min at 37°C plus 3 min at 95°C and then retrotranscribed by incubation with Moloney leukemia virus transcriptase (Invitrogen) and Primer Random mix (Roche, cat# 11034731001) for 60 min at 37°C plus 3 min at 95°C. The amplification reaction of both miRNAs and mRNA retrotranscribed samples was performed following the ΔΔCt routine (see details in: https://assets.thermofisher.com/TFS-Assets/LSG/manuals/4364016.pdf) in a TaqMan 7900HT Fast Real-Time PCR System (Applied Biosystems) using the TaqMan Universal PCR Master Mix, no AmpErase UNG (Fisher Scientific, cat#4324018) together with commercial specific FAM-MBG conjugated probe for XIAP mRNA (Life Technologies; cat#4331182; Rn01457299_m1) and for miR-199a-5p miRNA (gene expression-specific probe, TaqMan® MicroRNA assay cat#000498). 18S ribosomal RNA (for mRNA; Life Technologies, cat#4333760; Hs99999901_s1) and U6 RNA (for miRNA; TaqMan® MicroRNA assay cat#001973, Applied Biosystems) served as internal control). The reactions

 doi:10.20944/preprints202212.0020.v1

were programmed in the 9600 emulation mode, that is, first 10 min at 95°C, followed by 40 cycles of a two-step amplification run, comprising 15 s at 95°C, plus 1 min at 60°C.

Both miRNA and mRNA data were analyzed following the methods from Livak and Schmittgen [75]. Briefly, we determined the difference (ΔCt) between the cycle threshold of the target mRNA or miRNA and their respective endogenous loading controls and its associated variance following the standard propagation of error method from Headrick and col. [76]. Then, we compared the ΔCt value from the miR-199a-5p mimic condition with the ΔCt from the negative control sequence to calculate the ΔΔCt and the correspondent fold increase ($2^{\Delta\Delta}$Ct), indicating also the 95% confidence interval. Statistical analysis was performed using a one-way ANOVA with Tukey post hoc test.

4.6. Dual-luciferase reporter gene construction and 3'UTR Luciferase reporter assays

The wild type (wt) 3'UTR sequence of rat XIAP mRNA (XIAP 3'UTR-wt; NCBI Reference Sequence: NM_022231.2) containing the predicted binding site for rno-miR-199a-5p (nt 2255-2262) was obtained from total rat brain DNA extract by amplification by PCR (Table 3). The amplified sequence was subcloned into the T vector plasmid (pGEM-T-easy, Promega) and a pBKS vector (pBluescript, Stratagene). The 3'UTR sequence was validated by DNA sequencing (T7p and SP6). After amplification by and transformation in of *E.coli* super-competent cells (Thermo Scientific), the XIAP 3'UTR-wt sequence was inserted into the pmiRGLO Dual-luciferase miRNA Target Expression Vector (Promega, a scheme on the reporter construct is available at (http://www.addgene.org/vector-database/8236/]) between the SacI and XbaI restriction sites (pmiR-GloXIAP) using the FastDigest restriction enzymes (Thermo Scientific). Following a similar strategy as the QuikChange Site-Directed Mutagenesis (Thermo Scientific) a 3'UTRpoint mutant sequence (XIAP 3'UTR-mut) was generated by PCR using the XIAP 3'UTR-mut primers (See supplementary data 1) and the PfuI polymerase (Thermo Scientific), and the pBKS plasmid with the XIAP 3'UTR-wt subcloned serving as template after DpnI endonuclease restriction digestion (FastDigest, Thermo Scientific). After amplification by transformation in *E.coli* super-competent cells, the XIAP-3'UTR-mut fragment was inserted into pmiRGLO between the SacI and SalI restriction sites (pmiR-GloXIAP-MUT). Finally, we confirmed the sequence of both pmiRGLO 3'UTR-XIAP constructs by DNA sequencing using a specific forward 3' end luciferase primer.

C6 cells were grown at 80% confluence (10^4 cells per well in 96-well plate) and co-transfected with 50 nM of miR-199a-5p or negative control (cel-miR-67) mimics and 2 μg/mL of pmiR-Glo^{XIAP} or pmiR-Glo$^{XIAP\text{-}MUT}$, using the DharmaFECT Duo Transfection Reagent (Dharmacon). After 24 h, we measured the firefly luciferase to Renilla luciferase light emission ratio according to the manufacturer´s protocol (Dual-Luciferase Reporter Assay System, Promega) using a spectrophotometer plate reader (Infinite M200, Tecan Group LTD). Firefly emission data were normalized to Renilla load control levels and expressed as the firefly/Renilla ratio.

4.7. Immunoblotting assay.

C6 cells were cultured in a 6-well plate (2.5×10^5 cells per well). After reaching 80% confluence, cultures were transfected for 24 h with 50 nM of either the miR-199a-5p or negative control mimics. The endogenous levels of XIAP protein were measured using a standard immunoblot procedure. Briefly, total protein was extracted using mechanical detachment of the cells followed by lysis in RIPA lysis buffer (R0278; Sigma) supplemented with a protease inhibitor cocktail (Sigma), incubated for 30 min at 4°C and cleared by centrifugation (12.000 × g for 10 min at 4°C). Protein concentration of the lysates was quantified using the bicinchoninic acid method (ThermoFisher Scientific) following the manufacturer's protocol. Cell lysates were mixed with Laemmli buffer (2-mercaptoethanol, 0.1% (Sigma); bromophenol blue, 0.0005% (UBS Affimetrix); Glycerol, 10%; Sodium dodecyl sulfate (SDS), 2% and Tris-HCl, 63 mM (pH 6.8)) and boiled for 5 min at 100°C. After SDS-polyacrylamide gel electrophoresis (SDS-PAGE), proteins were transferred to polyvinylidene difluoride membranes (PVDF, Merk Millipore, Cat.# P2813). Then,

 doi:10.20944/preprints202212.0020.v1

membranes were blocked with 5% non-fat milk diluted in TBS-T buffer (Tris buffer saline (Fischer Scientific, Cat.# BP2471) plus 0.05% (v/v) Tween20 (Merk, Cat.# P9416)) and incubated overnight at 4°C with the appropriate specific antibodies diluted in blocking solution (see Table 4 for antibody concentrations). Afterwards, blots were incubated at RT for 90 min with the correspondent horseradish peroxidase (HRP)-conjugated secondary antibody (see Supplementary data 2) diluted in a blocking solution. Detection by enhanced chemiluminescence (ECL) was performed using SuperSignal West Pico chemiluminescent assay (Thermo Fisher Scientific) according to the manufacturer's instructions. Blot images were acquired using ImageScanner III and LabScan v6.0 software (GE Healthcare Bio-Sciences AB) and band intensities were measured using ImageJ software version 1.53f51 [77]. All employed antibodies recognized the specific band or bands of expected molecular weight for their target without detection of any non-specific bands.

4.8. Immunofluorescence

C6 cells were cultured over 12 mm round glass coverslips inside a 24-well plate (10^4 cells per well). After reaching 80% confluence, cultures were transfected for 24 h with 50 nM of either miR-199a-5p or negative control mimics. Then, cells were fixed with 4% paraformaldehyde for 20 min at room temperature (RT) and then permeabilized and blocked by incubation overnight at 4°C with blocking buffer (5% goat serum (Merk) and 0.2% Triton X-100 (Merk) in PBS 1x). Samples were then incubated for 2 h at RT in a solution of anti-XIAP antibody (1:500) diluted in blocking buffer, followed by three washes in PBS and incubation in a solution of secondary antibody Alexa Fluor 488 nm-conjugated rabbit anti-goat (1:500), diluted in blocking buffer. Finally, coverslips were mounted on glass slides employing Fluorescence Mounting Medium (DAKO North America Inc. Agilent Technologies Inc.) with 1:30000 of the fluorescent marker of nucleic acids 4',6-diamino-2-fenilindol for nuclei staining (DAPI, Merk). Preparations were imaged in an epifluorescence microscope (DM5000B, Leica Microsystem GmbH) with a 20x objective obtaining 5 images per sample. Using the object classification tools included in the detection tools QPath software vs 0.3.2 [78], we detected all cells present in the image through DAPI nuclei staining, measuring then the mean intensity of XIAP staining per cell. No XIAP staining was detected in controls without primary antibodies.

4.9. Fluorescence in situ Hybridization (FISH)

For FISH staining of miR-199a-5p in the spinal cord sections, we followed the protocol described by Søe et al. [79]. All the following solutions were diluted in autoclaved RNAse-free water (H2O-DEPC; water treated 24h with diethylpyrocarbonate (DEPC, 1:1000 in distilled water; Merk) and autoclaved before use). In brief, we thawed spinal cord sections and then treated them with proteinase K for 15 min at 37ºC (40 µg/mL in Tris/HCl 40 mM pH 7.4 with EDTA (1mM) and NaCl (1 mM)). To avoid non-specific ionic bindings, we treated the sections with an acetylation buffer for 10 min at RT (triethanolamine (1.3% (v/v), Merk), HCl (0.06% (v/v); Merk) and acetic anhydride (0.25% (v/v); Merk). Then we incubated sections in hybridization buffer (1x miRCURY LNA miRNA ISH buffer; Qiagen) for 30 min at 65ºC and then with either miR-199a-5p or negative control (cel-miR-67) probes (Eurogentec; Seraing, Belgium) diluted in hybridization buffer at 70 nM. We designed both probes following Søe et al. (2011) including LNA and 2'-O-Methyl nucleotides for RNA stabilization and conjugated with a digoxigenin in the 5' extreme (see Table 5 for probe sequences and modifications). Probes were denatured for 4 min at 80ºC and incubated with the sections for 1 h at 65ºC. Then, we sequentially washed cells in 75 mM, 15 mM, and 1.5 mM saline-sodium citrate solutions (SSC; Fisher) for 3 min at 65ºC each and a final wash in 1.5 mM SSC for 3 min at RT. For detection, we incubated the sections in blocking buffer (horse serum (5%) and BSA (1%) in PBS-T-DEPC) for 15 min at 37ºC and then with an alkaline phosphatase-conjugated sheep-anti-digoxigenin antibody (see details in table 1) for 20 min at 37ºC. Finally, we incubated the sections with the alkaline phosphatase subtract Vector Blue (Vector Laboratories) following the manufacturer's protocol.

 doi:10.20944/preprints202212.0020.v1

After FISH protocol, we carried out immunofluorescent staining for cell type detection to analyze miR-199a-5p expression in neurons. We incubated sections with specific cell marker antibody for neurons (anti-NeuN; see Table 4) diluted in blocking solution overnight at 4ºC. Then we washed sections in PBS and incubated them with the appropriate Alexa Fluor-conjugated secondary antibodies (see Supplementary data 3) also diluted in blocking solution, for 2h at RT. Finally, we mounted the stained sections with a Fluorescent Mounting Medium (DAKO) containing 1:30000 of DAPI. For expression analysis, we acquired images in an epifluorescence microscope with a x40 objective and analyzed them using ImageJ 1.51n software.

To determine the percentage of neural cells expressing miR-199a-5p we followed the method described in [33]. In brief, we determined the total neurons present in the grey matter and also, the neural cells in the white matter from each spinal cord section analyzed. Agreement upon two independent observers determined which cells were positive for miR-199a-5p staining.

4.10. Data Analysis

All data are expressed as mean ± SEM as indicated in figure legends. Statistical significance of the treatment effects was tested using paired or non-paired Student's t-test or an analysis of variance test (ANOVA) depending on the characteristics of the data. Normality and homoscedasticity of the data were assessed using Shapiro–Wilk and Bartlett or F tests, respectively, using the Shapiro.test, Bartlett.test, var.test functions of R. Mann–Whitney– Wilcoxon test was employed to substitute Student's t-test when data were deemed non-parametric (immunofluorescence data following miR-199a-5p over-expression). We employed Grubbs' test (also known as the extreme Studentized deviate test method, available online at https://www.graphpad.com/quickcalcs/grubbs1/) to search for outliers among the analysis data. Statistical analyses and graphics were carried out using Prism Software 5 (GraphPad Software Inc., La Jolla, CA, USA) and R statistical language (R Core Team 2014). Differences were considered statistically significant when the p-value < 0.05.

5. Conclusions

In the present study, we first validated that miR-199a-5p is a regulator of the antiapoptotic protein XIAP and provided evidence that the expression of miR-199a-5p is up-regulated after SCI in a neuronal heterogeneous spatial distribution whilst in a homogeneous white matter neural cells expression. This study provides new insight into the specific mechanisms of miR-199a-5p and XIAP in the apoptotic cell death after SCI that could be beneficial for the development of a therapeutic approach to SCI treatment.

Supplementary Materials: The following supporting information can be downloaded at: www.mdpi.com/

Author Contributions: Conceptualization, Teresa Muñoz-Galdeano and Rodrigo Maza; Data curation, Manuel Nieto-Díaz; Formal analysis, Teresa Muñoz-Galdeano, David Reigada, Manuel Nieto-Díaz and Rodrigo Maza; Funding acquisition, Teresa Muñoz-Galdeano and Rodrigo Maza; Investigation, Teresa Muñoz-Galdeano, María Gamarra, Manuel Nieto-Díaz and Rodrigo Maza; Methodology, Teresa Muñoz-Galdeano, David Reigada, Altea Soto, María Asunción Barreda-Manso and Rodrigo Maza; Writing – original draft, Teresa Muñoz-Galdeano and Rodrigo Maza; Writing – review & editing, Teresa Muñoz-Galdeano, David Reigada, María Gamarra, Altea Soto, María Asunción Barreda-Manso, Irene Novillo, Manuel Nieto-Díaz and Rodrigo Maza. All authors have revised and approved the final version of this article and express their agreement for all aspects of the present work in ensuring that questions related to the accuracy or integrity of any part of the work are appropriately investigated and resolved. All authors have read and agreed to the published version of the manuscript.

Funding: This research was funded by grants from the Fundación Tatiana Pérez de Guzmán el Bueno (Proyectos Neurociencia 2016) and the Council of Education, Culture, and Sports of the Regional Government of Castilla La Mancha (Spain) and Co-financed by the European Union (FEDER) "A way to make Europe" (project references SBPLY/17/000376 and SBPLY/21/180501/000097). M.

Asunción Barreda-Manso is funded by the Council of Health of the Regional Government of Castilla La Mancha (Spain), through the "Convocatoria de Ayudas Regionales a la Investigación en Biomedicina y Ciencias de la Salud", #II-2020_05. Altea Soto was funded by the Council of Education, Culture, and Sports of the Regional Government of Castilla La Mancha (Spain).

Institutional Review Board Statement: All experimental procedures were in accordance with the European Communities Council Directive 2010/63/EU, Spanish Royal Decree 53/2013 (experimental animal use regulation), and Order ECC/566/ 2015 (regulation of personnel formation in animal experimentation) and were approved by the Hospital Nacional de Parapléjicos Animal Care and Use Committee (project ref #153BCEEA/2016).

Informed Consent Statement: Not applicable.

Data Availability Statement: Not applicable.

Acknowledgments: We thank the Fundación del Hospital Nacional de Parapléjicos para la Investigación y la Integración (FUHNPAIIN) and the microscopy and animal facilities from the Research Unit of the Hospital Nacional de Parapléjicos (Toledo, Spain) for their technical and logistic support.

Conflicts of Interest: The authors declare no conflict of interest.

References

1. Devivo: M. J. 2012. Epidemiology of traumatic spinal cord injury: Trends and future implications. In *Spinal Cord*, 50:365–372. Spinal Cord. https://doi.org/10.1038/sc.2011.178.
2. Alizadeh, Arsalan, Scott Matthew Dyck, and Soheila Karimi-Abdolrezaee. 2019. Traumatic Spinal Cord Injury: An Overview of Pathophysiology, Models and Acute Injury Mechanisms. *Frontiers in Neurology* 10. Frontiers. https://doi.org/10.3389/fneur.2019.00282.
3. Ahuja, Christopher S., Jefferson R. Wilson, Satoshi Nori, Mark R. N. Kotter, Claudia Druschel, Armin Curt, and Michael G. Fehlings. 2017. Traumatic spinal cord injury. *Nature Reviews Disease Primers* 3. Nature Publishing Group: 1–21. https://doi.org/10.1038/nrdp.2017.18.
4. Grossman, S. D., L. J. Rosenberg, and J. R. Wrathall. 2001. Temporal-spatial pattern of acute neuronal and glial loss after spinal cord contusion. *Experimental Neurology* 168: 273–282. https://doi.org/10.1006/exnr.2001.7628.
5. Barbon, Alessandro, Fabio Fumagalli, Luca Caracciolo, Laura Madaschi, Elena Lesma, Cristina Mora, Stephana Carelli, et al. 2010. Acute spinal cord injury persistently reduces R/G RNA editing of AMPA receptors. *Journal of Neurochemistry* 114: 397–407. https://doi.org/10.1111/j.1471-4159.2010.06767.x.
6. Nakae, Aya, Kunihiro Nakai, Tatsuya Tanaka, Ko Hosokawa, and Takashi Mashimo. 2013. Serotonin 2C receptor alternative splicing in a spinal cord injury model. *Neuroscience Letters* 532: 49–54. https://doi.org/10.1016/j.neulet.2012.10.034.
7. Anilkumar, Ujval, and Jochen H. M. Prehn. 2014. Anti-apoptotic BCL-2 family proteins in acute neural injury. *Frontiers in Cellular Neuroscience* 8. Frontiers Research Foundation: 281. https://doi.org/10.3389/fncel.2014.00281.
8. Dasari, Venkata Ramesh, Krishna Kumar Veeravalli, Andrew J. Tsung, Christopher S. Gondi, Meena Gujrati, Dzung H. Dinh, and Jasti S. Rao. 2009. Neuronal apoptosis is inhibited by cord blood stem cells after spinal cord injury. *Journal of Neurotrauma* 26. Mary Ann Liebert, Inc. 140 Huguenot Street, 3rd Floor New Rochelle, NY 10801 USA: 2057–2069. https://doi.org/10.1089/neu.2008.0725.
9. Tu, Huailu, and Max Costa. 2020. XIAP's Profile in Human Cancer. *Biomolecules* 10: 1493. https://doi.org/10.3390/biom10111493.
10. Roy, N., Q. L. Deveraux, R. Takahashi, G. S. Salvesen, and J. C. Reed. 1997. The c-IAP-1 and c-IAP-2 proteins are direct inhibitors of specific caspases. *The EMBO journal* 16: 6914–6925. https://doi.org/10.1093/emboj/16.23.6914.
11. Hollville, Emilie, Selena E. Romero, and Mohanish Deshmukh. 2019. Apoptotic cell death regulation in neurons. *The FEBS Journal* 286. Blackwell Publishing Ltd: 3276–3298. https://doi.org/10.1111/febs.14970.
12. Zhang, Ning, Ying Yin, Sheng-Jie Xu, Yong-Ping Wu, and Wei-Shan Chen. 2012. Inflammation & apoptosis in spinal cord injury. *The Indian Journal of Medical Research* 135: 287–296.
13. Kang, Young Ji, Mi Jang, Yun Kyung Park, Sunghyun Kang, Kwang-Hee Bae, Sayeon Cho, Chong-Kil Lee, Byoung Chul Park, Seung-Wook Chi, and Sung Goo Park. 2010. Molecular interaction between HAX-1 and XIAP inhibits apoptosis. *Biochemical and Biophysical Research Communications* 393: 794–799. https://doi.org/10.1016/j.bbrc.2010.02.084.
14. Xu, Jiheng, Xiaohui Hua, Rui Yang, Honglei Jin, Jingxia Li, Junlan Zhu, Zhongxian Tian, et al. 2019. XIAP Interaction with E2F1 and Sp1 via its BIR2 and BIR3 domains specific activated MMP2 to promote bladder cancer invasion. *Oncogenesis* 8. Nature Publishing Group: 1–9. https://doi.org/10.1038/s41389-019-0181-8.
15. Harlin, H., S. B. Reffey, C. S. Duckett, T. Lindsten, and C. B. Thompson. 2001. Characterization of XIAP-deficient mice. *Molecular and Cellular Biology* 21: 3604–3608. https://doi.org/10.1128/MCB.21.10.3604-3608.2001.
16. Blancas, Sugela, Rut Fadó, José Rodriguez-Alvarez, and Julio Morán. 2014. Endogenous XIAP, but not other members of the inhibitory apoptosis protein family modulates cerebellar granule neurons survival. *International Journal of Developmental Neuroscience: The Official Journal of the International Society for Developmental Neuroscience* 37: 26–35. https://doi.org/10.1016/j.ijdevneu.2014.06.006.

17. West, Tim, Madeliene Stump, Gregory Lodygensky, Jeff J. Neil, Mohanish Deshmukh, and David M. Holtzman. 2009. Lack of X-linked inhibitor of apoptosis protein leads to increased apoptosis and tissue loss following neonatal brain injury. *ASN neuro* 1. https://doi.org/10.1042/AN20090005.
18. Potts, Patrick Ryan, Shweta Singh, Malia Knezek, Craig B. Thompson, and Mohanish Deshmukh. 2003. Critical function of endogenous XIAP in regulating caspase activation during sympathetic neuronal apoptosis. *Journal of Cell Biology* 163. J Cell Biol: 789–799. https://doi.org/10.1083/jcb.200307130.
19. Perrelet, D., A. Ferri, P. Liston, P. Muzzin, R. G. Korneluk, and A. C. Kato. 2002. IAPs are essential for GDNF-mediated neuroprotective effects in injured motor neurons in vivo. *Nature Cell Biology* 4. Nature Publishing Group: 175–179. https://doi.org/10.1038/ncb751.
20. Keane, Robert W., Susan Kraydieh, George Lotocki, John R. Bethea, Stanislaw Krajewski, John C. Reed, and W. Dalton Dietrich. 2001. Apoptotic and Anti-Apoptotic Mechanisms Following Spinal Cord Injury. *Journal of Neuropathology & Experimental Neurology* 60. American Association of Neuropathologists Inc.: 422–429. https://doi.org/10.1093/jnen/60.5.422.
21. de Rivero Vaccari, Juan Pablo, W Dalton Dietrich, and Robert W Keane. 2014. Activation and regulation of cellular inflammasomes: gaps in our knowledge for central nervous system injury. *Journal of Cerebral Blood Flow & Metabolism* 34: 369–375. https://doi.org/10.1038/jcbfm.2013.227.
22. Reigada, D., M. Nieto-Díaz, R. Navarro-Ruiz, M. J. Caballero-López, A. del Águila, T. Muñoz-Galdeano, and R. M. Maza. 2015. Acute administration of ucf-101 ameliorates the locomotor impairments induced by a traumatic spinal cord injury. *Neuroscience* 300. Elsevier Ltd: 404–417. https://doi.org/10.1016/j.neuroscience.2015.05.036.
23. Xu, D., Y. Bureau, D. C. McIntyre, D. W. Nicholson, P. Liston, Y. Zhu, W. G. Fong, S. J. Crocker, R. G. Korneluk, and G. S. Robertson. 1999. Attenuation of ischemia-induced cellular and behavioral deficits by X chromosome-linked inhibitor of apoptosis protein overexpression in the rat hippocampus. *The Journal of Neuroscience: The Official Journal of the Society for Neuroscience* 19: 5026–5033.
24. MicroRNA Dysregulation in the Spinal Cord following Traumatic Injury. 2021. https://journals.plos.org/plosone/article?id=10.1371/journal.pone.0034534. Accessed June 8.
25. Nieto-Díaz, Manuel, Francisco José Esteban, David Reigada, Teresa Muñoz-Galdeano, Mónica Yunta, Marcos Caballero-López, Rosa Navarro-Ruiz, Ángela del Águila, and Rodrigo Martínez Maza. 2014. MicroRNA dysregulation in spinal cord injury: causes, consequences and therapeutics. *Frontiers in Cellular Neuroscience* 8. Frontiers. https://doi.org/10.3389/fncel.2014.00053.
26. Selbach, Matthias, Björn Schwanhäusser, Nadine Thierfelder, Zhuo Fang, Raya Khanin, and Nikolaus Rajewsky. 2008. Widespread changes in protein synthesis induced by microRNAs. *Nature* 455. Nature Publishing Group: 58–63. https://doi.org/10.1038/nature07228.
27. Sayed, Danish, and Maha Abdellatif. 2011. MicroRNAs in development and disease. *Physiological Reviews* 91: 827–887. https://doi.org/10.1152/physrev.00006.2010.
28. Su, Zhenyi, Zuozhang Yang, Yongqing Xu, Yongbin Chen, and Qiang Yu. 2015. MicroRNAs in apoptosis, autophagy and necroptosis. *Oncotarget* 6: 8474–8490. https://doi.org/10.18632/oncotarget.3523.
29. Hata, Akiko, and Judy Lieberman. 2015. Dysregulation of microRNA biogenesis and gene silencing in cancer. *Science Signaling* 8: re3. https://doi.org/10.1126/scisignal.2005825.
30. Zhang, Haocong, and Yan Wang. 2016. Identification of molecular pathway changes after spinal cord injury by microarray analysis. *Journal of Orthopaedic Surgery and Research* 11. https://doi.org/10.1186/s13018-016-0437-3.
31. Liu, Yugang, Ying Wang, Zhaowei Teng, Xiufeng Zhang, Min Ding, Zhaojun Zhang, Junli Chen, and Yanli Xu. 2016. DNA Microarray Analysis in Screening Features of Genes Involved in Spinal Cord Injury. *Medical Science Monitor : International Medical Journal of Experimental and Clinical Research* 22: 1571–1581. https://doi.org/10.12659/MSM.895889.
32. Squair, Jordan W, Seth Tigchelaar, Kyung-Mee Moon, Jie Liu, Wolfram Tetzlaff, Brian K Kwon, Andrei V Krassioukov, Christopher R West, Leonard J Foster, and Michael A Skinnider. 2018. Integrated systems analysis reveals conserved gene networks underlying response to spinal cord injury. *eLife* 7. eLife Sciences Publications, Ltd: e39188. https://doi.org/10.7554/eLife.39188.
33. Maza, Rodrigo M., María Asunción Barreda-Manso, David Reigada, Ágata Silván, Teresa Muñoz-Galdeano, Altea Soto, Ángela del Águila, and Manuel Nieto-Díaz. 2022. MicroRNA-138-5p Targets Pro-Apoptotic Factors and Favors Neural Cell Survival: Analysis in the Injured Spinal Cord. *Biomedicines* 10. Multidisciplinary Digital Publishing Institute: 1559. https://doi.org/10.3390/biomedicines10071559.
34. Xu, Zhongyang, Kefeng Zhang, Qian Wang, and Yanping Zheng. 2019. MicroRNA-124 improves functional recovery and suppresses Bax-dependent apoptosis in rats following spinal cord injury. *Molecular Medicine Reports* 19: 2551–2560. https://doi.org/10.3892/mmr.2019.9904.
35. Jiang, Dongdong, Fangyi Gong, Xuhui Ge, Chengtang Lv, Chenyu Huang, Shuang Feng, Zheng Zhou, et al. 2020. Neuron-derived exosomes-transmitted miR-124-3p protect traumatically injured spinal cord by suppressing the activation of neurotoxic microglia and astrocytes. *Journal of Nanobiotechnology* 18: 105. https://doi.org/10.1186/s12951-020-00665-8.
36. Sabirzhanov, Boris, Jessica Matyas, Marina Coll-Miro, Laina Lijia Yu, Alan I. Faden, Bogdan A. Stoica, and Junfang Wu. 2019. Inhibition of microRNA-711 limits angiopoietin-1 and Akt changes, tissue damage, and motor dysfunction after contusive spinal cord injury in mice. *Cell Death & Disease* 10. Nature Publishing Group: 1–14. https://doi.org/10.1038/s41419-019-2079-y.
37. Sabirzhanov, Boris, Zaorui Zhao, Bogdan A. Stoica, David J. Loane, Junfang Wu, Carlos Borroto, Susan G. Dorsey, and Alan I. Faden. 2014. Downregulation of miR-23a and miR-27a following experimental traumatic brain injury induces neuronal cell death through activation of proapoptotic Bcl-2 proteins. *The Journal of Neuroscience: The Official Journal of the Society for Neuroscience* 34: 10055–10071. https://doi.org/10.1523/JNEUROSCI.1260-14.2014.

 doi:10.20944/preprints202212.0020.v1

38. Liu, Xing, Xintao Cui, Guangwei Guan, Ying Dong, and Zhenyu Zhang. 2020. microRNA-192-5p is involved in nerve repair in rats with peripheral nerve injury by regulating XIAP. *Cell Cycle* 19. Taylor and Francis Inc.: 326–338. https://doi.org/10.1080/15384101.2019.1710916.
39. Siegel, Chad, Jun Li, Fudong Liu, Sharon E. Benashski, and Louise D. McCullough. 2011. miR-23a regulation of X-linked inhibitor of apoptosis (XIAP) contributes to sex differences in the response to cerebral ischemia. *Proceedings of the National Academy of Sciences of the United States of America* 108. National Academy of Sciences: 11662–11667. https://doi.org/10.1073/pnas.1102635108.
40. Hutchison, Emmette R., Elisa M. Kawamoto, Dennis D. Taub, Ashish Lal, Kotb Abdelmohsen, Yongqing Zhang, William H. Wood, et al. 2013. Involvement of miR-181 in Neuroinflammatory Responses of Astrocytes. *Glia* 61: 1018–1028. https://doi.org/10.1002/glia.22483.
41. Kertesz, Michael, Nicola Iovino, Ulrich Unnerstall, Ulrike Gaul, and Eran Segal. 2007. The role of site accessibility in microRNA target recognition. *Nature Genetics* 39. Nature Publishing Group: 1278–1284. https://doi.org/10.1038/ng2135.
42. Yunta, Mónica, Manuel Nieto-Díaz, Francisco J. Esteban, Marcos Caballero-López, Rosa Navarro-Ruíz, David Reigada, D. Wolfgang Pita-Thomas, Ángela del Águila, Teresa Muñoz-Galdeano, and Rodrigo M. Maza. 2012. MicroRNA Dysregulation in the Spinal Cord following Traumatic Injury. *PLOS ONE* 7. Public Library of Science: e34534. https://doi.org/10.1371/journal.pone.0034534.
43. Liu, Nai-Kui, Xiao-Fei Wang, Qing-Bo Lu, and Xiao-Ming Xu. 2009. Altered microRNA expression following traumatic spinal cord injury. *Experimental Neurology* 219: 424–429. https://doi.org/10.1016/j.expneurol.2009.06.015.
44. Atif, Hamna, and Steven D Hicks. 2019. A Review of MicroRNA Biomarkers in Traumatic Brain Injury. *Journal of Experimental Neuroscience* 13. SAGE Publications Ltd STM: 1179069519832286. https://doi.org/10.1177/1179069519832286.
45. Bhalala, Oneil G., Maya Srikanth, and John A. Kessler. 2013. The emerging roles of microRNAs in CNS injuries. *Nature reviews. Neurology* 9: 328–339. https://doi.org/10.1038/nrneurol.2013.67.
46. Lei, Ping, Yaohua Li, Xin Chen, Shuyuan Yang, and Jianning Zhang. 2009. Microarray based analysis of microRNA expression in rat cerebral cortex after traumatic brain injury. *Brain Research* 1284: 191–201. https://doi.org/10.1016/j.brainres.2009.05.074.
47. Casha, S., W. R. Yu, and M. G. Fehlings. 2001. Oligodendroglial apoptosis occurs along degenerating axons and is associated with FAS and p75 expression following spinal cord injury in the rat. *Neuroscience* 103: 203–218. https://doi.org/10.1016/s0306-4522(00)00538-8.
48. Vaccari, Juan Pablo de Rivero, George Lotocki, Alex E. Marcillo, W. Dalton Dietrich, and Robert W. Keane. 2008. A Molecular Platform in Neurons Regulates Inflammation after Spinal Cord Injury. *Journal of Neuroscience* 28. Society for Neuroscience: 3404–3414. https://doi.org/10.1523/JNEUROSCI.0157-08.2008.
49. Jiang, Xue-Ping, Wen-Bing Ai, Lin-Yan Wan, Yan-Qiong Zhang, and Jiang-Feng Wu. 2017. The roles of microRNA families in hepatic fibrosis. *Cell & Bioscience* 7. https://doi.org/10.1186/s13578-017-0161-7.
50. Lagos-Quintana, Mariana, Reinhard Rauhut, Jutta Meyer, Arndt Borkhardt, and Thomas Tuschl. 2003. New microRNAs from mouse and human. *RNA (New York, N.Y.)* 9: 175–179. https://doi.org/10.1261/rna.2146903.
51. Liu, Gang, Megan Ryan Detloff, Kassi N. Miller, Lauren Santi, and John D. Houlé. 2012. Exercise modulates microRNAs that affect the PTEN/mTOR pathway in rats after spinal cord injury. *Experimental Neurology* 233. Special Issue: Stress and Neurological Disease: 447–456. https://doi.org/10.1016/j.expneurol.2011.11.018.
52. Landgraf, Pablo, Mirabela Rusu, Robert Sheridan, Alain Sewer, Nicola Iovino, Alexei Aravin, Sébastien Pfeffer, et al. 2007. A mammalian microRNA expression atlas based on small RNA library sequencing. *Cell* 129: 1401–1414. https://doi.org/10.1016/j.cell.2007.04.040.
53. Lim, Lee P., Nelson C. Lau, Earl G. Weinstein, Aliaa Abdelhakim, Soraya Yekta, Matthew W. Rhoades, Christopher B. Burge, and David P. Bartel. 2003. The microRNAs of Caenorhabditis elegans. *Genes & Development* 17: 991–1008. https://doi.org/10.1101/gad.1074403.
54. Strickland, E. R., M. A. Hook, S. Balaraman, J. R. Huie, J. W. Grau, and R. C. Miranda. 2011. MicroRNA dysregulation following spinal cord contusion: implications for neural plasticity and repair. *Neuroscience* 186: 146–160. https://doi.org/10.1016/j.neuroscience.2011.03.063.
55. Zhang, Tao, Shuangfei Ni, Zixiang Luo, Ye Lang, Jianzhong Hu, and Hongbin Lu. 2019. The protective effect of microRNA-21 in neurons after spinal cord injury. *Spinal Cord* 57. Nature Publishing Group: 141–149. https://doi.org/10.1038/s41393-018-0180-1.
56. Xu, Guanghui, Rongguang Ao, Zhongzheng Zhi, Jianbo Jia, and Baoqing Yu. 2019. miR-21 and miR-19b delivered by hMSC-derived EVs regulate the apoptosis and differentiation of neurons in patients with spinal cord injury. *Journal of Cellular Physiology* 234: 10205–10217. https://doi.org/10.1002/jcp.27690.
57. Kang, Jian, Zhenhuan Li, Zhongzheng Zhi, Shiqiang Wang, and Guanghui Xu. 2019. MiR-21 derived from the exosomes of MSCs regulates the death and differentiation of neurons in patients with spinal cord injury. *Gene Therapy* 26: 491–503. https://doi.org/10.1038/s41434-019-0101-8.
58. Gao, Zhengchao, Yingjie Zhao, Xijing He, Zikuan Leng, Xiaoqian Zhou, Hui Song, Rui Wang, et al. 2020. Transplantation of sh-miR-199a-5p-Modified Olfactory Ensheathing Cells Promotes the Functional Recovery in Rats with Contusive Spinal Cord Injury. *Cell Transplantation* 29. SAGE Publications Inc: 0963689720916173. https://doi.org/10.1177/0963689720916173.
59. Zhang, Zhong, Jian Wang, Zongbin Song, Yunjiao Wang, Zhigang Cheng, Qulian Guo, E. Wang, Yanping Jian, and Lei Wu. 2021. Downregulation of microRNA-199a-5p alleviated lidocaine-induced sensory dysfunction and spinal cord myelin lesions in a rat model. *Toxicology Letters* 336: 1–10. https://doi.org/10.1016/j.toxlet.2020.11.001.

60. Zhou, Qian, Ming-Ming Zhang, Min Liu, Zhi-Gang Tan, Qi-Lin Qin, and Yu-Gang Jiang. 2021. LncRNA XIST sponges miR-199a-3p to modulate the Sp1/LRRK2 signal pathway to accelerate Parkinson's disease progression. *Aging (Albany NY)* 13: 4115–4137. https://doi.org/10.18632/aging.202378.
61. Bao, Ning, Bo Fang, Huangwei Lv, Yanhua Jiang, Fengshou Chen, Zhilin Wang, and Hong Ma. 2018. Upregulation of miR-199a-5p Protects Spinal Cord Against Ischemia/Reperfusion-Induced Injury via Downregulation of ECE1 in Rat. *Cellular and Molecular Neurobiology* 38: 1293–1303. https://doi.org/10.1007/s10571-018-0597-2.
62. Gao, Lu, Xuehua Pu, Yujing Huang, and Jing Huang. 2019. MicroRNA-340-5p relieved chronic constriction injury-induced neuropathic pain by targeting Rap1A in rat model. *Genes & Genomics* 41: 713–721. https://doi.org/10.1007/s13258-019-00802-0.
63. Jiang, Hui, Jie Ni, Yan Zheng, and Yun Xu. 2021. Knockdown of lncRNA SNHG14 alleviates LPS-induced inflammation and apoptosis of PC12 cells by regulating miR-181b-5p. *Experimental and Therapeutic Medicine* 21: 497. https://doi.org/10.3892/etm.2021.9928.
64. Zhang, Meng, Lin Wang, Sihua Huang, and Xijing He. 2021. Exosomes with high level of miR-181c from bone marrow-derived mesenchymal stem cells inhibit inflammation and apoptosis to alleviate spinal cord injury. *Journal of Molecular Histology* 52: 301–311. https://doi.org/10.1007/s10735-020-09950-0.
65. Li, Feng, Jing Liang, Hua Tong, Shuai Zhu, and Dongfang Tang. 2020. Inhibition of microRNA-199a-5p ameliorates oxygen-glucose deprivation/reoxygenation-induced apoptosis and oxidative stress in HT22 neurons by targeting Brg1 to activate Nrf2/HO-1 signalling. *Clinical and Experimental Pharmacology and Physiology* 47: 1020–1029. https://doi.org/10.1111/1440-1681.13265.
66. Zhong, Wei, Yong-Chang Li, Qian-Yi Huang, and Xiang-Qi Tang. 2020. lncRNA ANRIL Ameliorates Oxygen and Glucose Deprivation (OGD) Induced Injury in Neuron Cells via miR-199a-5p/CAV-1 Axis. *Neurochemical Research* 45: 772–782. https://doi.org/10.1007/s11064-019-02951-w.
67. Zhang, Xianghui, and Guan'en Zhou. 2020. MiR-199a-5p inhibition protects cognitive function of ischemic stroke rats by AKT signaling pathway. *American Journal of Translational Research* 12: 6549–6558.
68. Xie, Yili, Lisa A. Tobin, Jordi Camps, Danny Wangsa, Jianhui Yang, Mahadev Rao, Erika Witasp, et al. 2013. MicroRNA-24 regulates XIAP to reduce the apoptosis threshold in cancer cells. *Oncogene* 32: 2442–2451. https://doi.org/10.1038/onc.2012.258.
69. Jonas, Stefanie, and Elisa Izaurralde. 2015. Towards a molecular understanding of microRNA-mediated gene silencing. *Nature Reviews Genetics* 16: 421–433. https://doi.org/10.1038/nrg3965.
70. Alexiou, Panagiotis, Manolis Maragkakis, Giorgos L. Papadopoulos, Martin Reczko, and Artemis G. Hatzigeorgiou. 2009. Lost in translation: an assessment and perspective for computational microRNA target identification. *Bioinformatics* 25: 3049–3055. https://doi.org/10.1093/bioinformatics/btp565.
71. Witkos, T. M., E. Koscianska, and W. J. Krzyzosiak. 2011. Practical Aspects of microRNA Target Prediction. *Current Molecular Medicine* 11: 93–109. https://doi.org/10.2174/156652411794859250.
72. Zuker, Michael. 2003. Mfold web server for nucleic acid folding and hybridization prediction. *Nucleic Acids Research* 31: 3406–3415. https://doi.org/10.1093/nar/gkg595.
73. Basso, D. M., M. S. Beattie, and J. C. Bresnahan. 1995. A sensitive and reliable locomotor rating scale for open field testing in rats. *Journal of Neurotrauma* 12: 1–21. https://doi.org/10.1089/neu.1995.12.1.
74. Statistical power analyses using G*Power 3.1: Tests for correlation and regression analyses | SpringerLink. 2022. https://link.springer.com/article/10.3758/BRM.41.4.1149. Accessed September 28.
75. Livak, K. J., and T. D. Schmittgen. 2001. Analysis of relative gene expression data using real-time quantitative PCR and the 2(-Delta Delta C(T)) Method. *Methods (San Diego, Calif.)* 25: 402–408. https://doi.org/10.1006/meth.2001.1262.
76. Headrick, Todd C. 2009. *Statistical Simulation: Power Method Polynomials and Other Transformations*. New York: Chapman and Hall/CRC. https://doi.org/10.1201/9781420064919.
77. Schneider, Caroline A., Wayne S. Rasband, and Kevin W. Eliceiri. 2012. NIH Image to ImageJ: 25 years of image analysis. *Nature Methods* 9. Nature Publishing Group: 671–675. https://doi.org/10.1038/nmeth.2089.
78. Bankhead, Peter, Maurice B. Loughrey, José A. Fernández, Yvonne Dombrowski, Darragh G. McArt, Philip D. Dunne, Stephen McQuaid, et al. 2017. QuPath: Open source software for digital pathology image analysis. *Scientific Reports* 7. Nature Publishing Group: 16878. https://doi.org/10.1038/s41598-017-17204-5.
79. Søe, Martin J., Trine Møller, Martin Dufva, and Kim Holmstrøm. 2011. A Sensitive Alternative for MicroRNA In Situ Hybridizations Using Probes of 2'-O-Methyl RNA + LNA. *Journal of Histochemistry and Cytochemistry* 59: 661–672. https://doi.org/10.1369/0022155411409411.